Earthq Eng & Eng Vib (2020) 19: 573-582 **DOI**: https://doi.org/10.1007/s11803-020-0581-y

Effects of soil dynamic response on post-earthquake deformation of slopes based on nested Newmark model

Zhou Zheng[1†], Gao Yufeng[1‡], Zhang Fei[1§], Song Jian[1*] and Zou Degao[2‡]

1. *Key Laboratory of Ministry of Education for Geomechanics and Embankment Engineering, Hohai University, Nanjing 210098, China*

2. *The State Key Laboratory of Coastal and Offshore Engineering, Dalian University of Technology, Dalian 116024, China*

Abstract: Nested Newmark model (NNM) can obtain the post-earthquake profile of the slopes in limit equilibrium or limit analysis method. The purpose of this study is to extend the NNM from the limit equilibrium method to a limit analysis method, and then involve the dynamic response of slopes into the prediction of the permanent displacement based on decoupled analysis. Parametric studies are carried out to further investigate the influences of slope height, soil shear wave velocity and input ground motion. The calculated results indicate that neglecting the dynamic response of slopes can underestimate the post-earthquake displacements. As the slope height increases or shear wave velocity reduces, the underestimation is more significant. At the fundamental natural period of the site, the underestimation is particularly remarkable. For induced earthquake waves with a small value of mean period, the influence of the dynamic response can be ignored when the fundamental period deviates from the mean period.

Keywords: slopes; earthquakes; permanent displacement; Newmark; soil dynamic response

1 Introduction

Earthquake-induced landslides are very common in seismic areas and the evaluation of slope stability needs to be given more attention. The approach of seismic assessments for slope stability can be divided into three main categories: pseudo-static method (e.g., Terzaghi, 1950; Sarma and Bhave, 1974), Newmark sliding block analysis (e.g., Newmark, 1965; Sarma, 1975), and stress-deformation analysis (e.g., Seed *et al*., 1975; Lee *et al*., 1974). The traditional pseudo-static method carries out the limit equilibrium (LE) or limit analysis (LA) to obtain the factor of safety for a given peak acceleration and neglects the acceleration-time history of the seismicity. The Newmark method can determine the permanent displacement of the slope during the earthquake. Furthermore, conducting dynamic finite-element (FE) or finite-difference (FD) analyses (e.g., Serff *et al*., 1976; Chugh *et al*., 2006) can obtain the stress and strain results of the slopes induced by earthquakes. However, the accuracy of the numerical results depends on the soil dynamic constitutive and boundary conditions. The estimation of permanent displacement of a slope based on the Newmark method bridges the gap between the simplified pseudo-static method and complicated stress-deformation analysis.

The classic Newmark method originates from the single rigid sliding block for seismic analysis of an earth dam and its results have been validated with laboratory model tests (e.g., Goodman and Seed, 1966; Wartman *et al*., 2005). Through dynamic centrifuge model tests, Kutter and James (1989) found a deep rotational failure surface in a clay embankment. The Newmark method was developed to determine the displacement using a log-spiral surface in LE or LA (e.g., Ling and Leshchinsky, 1995; You and Michalowski, 1999; Aminpour *et al*., 2018; Yang *et al*., 2020). However, the rotational failure mechanism was still limited to sliding of a rigid body. Experimental results (Wartman *et al*., 2005; Kutter and James, 1989) demonstrated general deformations which exhibit multiple failure surfaces or regions of internal shear movements. To include general deformation in the Newmark method, Leshchinsky (2018) recently proposed a Nested Newmark model (NNM) to predict the post-earthquake displacement profiles of slopes using both of planar and rotational failure surfaces in LE. The

Correspondence to: Gao Yufeng, Key Laboratory of Ministry of Education for Geomechanics and Embankment Engineering, Hohai University, Nanjing 210098, China
Tel: +86-025-83787287
E-mail: yfgao66@163.com

† PhD Candidate; ‡Professor; § Associate Professor;*Lecturer

Supported by: National Natural Science Foundation of China under Grant Nos. 41630638 and 41602280, the National Key Research and Development Program of China under Grant No. 2016YFC0800205, the Program of Introducing Talents of Discipline to Universities 111 Project under Grant No. B13024

Received January 24, 2019; **Accepted** November 26, 2019

effects of multiple slip surfaces and dispersed regions of internal shear movement are considered in NNM.

The influence of slope response on the post-earthquake deformation was observed in some shaking table tests (Hong *et al*., 2005; Lin and Wang, 2006) and numerical simulations (Boukovalas, 2005; Dai *et al*., 2019; Zhang *et al*., 2018). Through comparisons of the seismic displacements obtained from different Newmark methods, Jibson (2011) found that the assumption of rigid-block sliding could yield an unconservative estimation on the displacement due to the flexibility of the earth structures. The dynamic response of soil slopes should be considered by the seismic assessment. Makdisi and Seed (1977) extended the Newmark procedure with a decoupled analysis, in which the computation of the dynamic analysis and the displacement were performed independently. To provide more appropriate dynamic analysis for application, Rathje and Bray (2001) carried out one-dimensional (1D) and two-dimensional (2D) dynamic response analyses of earth structures and demonstrated that 1D analysis can provide a reasonably conservative estimate of the seismic loading and earthquake-induced permanent displacement for deep sliding surfaces. However, their dynamic response analyses were limited to one-block sliding. The purpose of this study is to include the 1D dynamic response analyses into NNM. In the framework of LA, the log-spiral failure surface is employed here to determine the post-earthquake displacement profiles of soil slopes. Parametric studies are performed to investigate the influence of slope height, soil shear stiffness, and input motions on the deformation.

2 Methodology

In the framework of the Newmark method, Leshchinsky (2018) employed the LE approach to determine the post-earthquake profile of the slopes subjected to translational and rotational failure. As presented in Baker and Garber (1978), using the variational extremization of the factor of safety obtained the most critical failure surface, which was defined as a log-spiral. Leshchinsky *et al*. (1985) presented the equivalence between the variational LE approach and the kinematic approach of LA based on the upper-bound (UB) theorem of plasticity. This study involves the log-spiral failure surface in NNM and then determines the seismic displacements of earth slopes.

Figure 1 represents a homogeneous soil slope model subjected to pseudo-static seismic forces at the verge of failure. The inclination of the slope is described by angle b; the height of the slope is defined as H; and the soil is characterized by internal friction angle φ, cohesion c, and unit soil weight γ. First, conducting the pseudo-static approach can obtain the yield acceleration and the corresponding critical slip surface. The sliding body ABC rotates about the center O along a log-spiral AC passing through the slope toe. The log-spiral AC is expressed as

$$r = r_0 \mathrm{e}^{(\theta-\theta_0)\tan\varphi} \tag{1}$$

where r_0 = distance between center O and point A; θ_0 = angle between line OA and a horizontal line; and θ_h = angle between OC and horizontal line.

Based on the UB theorem, equating the rate of work done by the external forces (i.e., soil gravity weight and seismic forces) to the rate of the energy dissipation along the slip surface can yield the energy balance

$$W_\gamma + W_s = D \tag{2}$$

where W_γ = rate of work done by soil weight, W_s = rate of work done by the pseudo-static seismic load which defined by seismic coefficient k; and D = rate of internal energy dissipation for the sliding body ABC. The work rate W_γ can be calculated as the work rate of fictitious block OCA minus the work rates of the blocks AOB, BOC

$$W_\gamma = W_{\gamma 1} - W_{\gamma 2} - W_{\gamma 3} = \gamma\omega r_0^3 f_w \tag{3}$$

where $W_{\gamma 1}$, $W_{\gamma 2}$, $W_{\gamma 3}$ = the rate of work done by the soil weight of OCA, AOB, BOC respectively; and f_w = the function coefficient of β, θ_0, θ_h; ω = angular velocity. Similarly, the rate of work done by seismic forces S can be written as

$$W_s = W_{s1} - W_{s2} - W_{s3} = k\gamma\omega r_0^3 f_s \tag{4}$$

where W_{s1}, W_{s2}, W_{s3} = the rates of work done by the seismic forces on OCA, AOB, BOC respectively; and f_s = the function coefficient of β, θ_0, θ_h. In terms of the principal strain rates, the dissipation within the slip surface can be expressed as

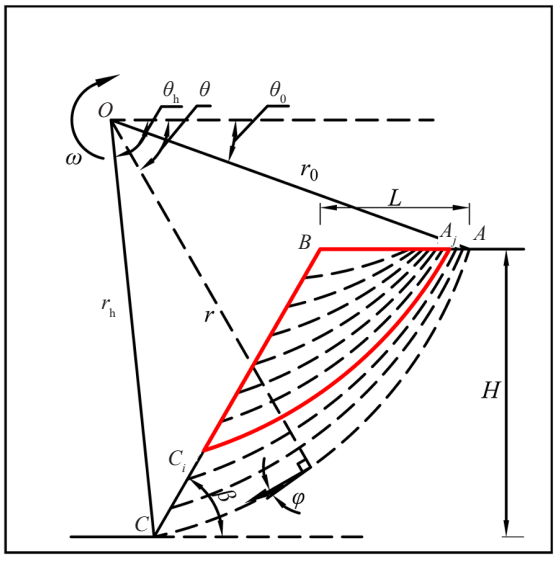

Fig. 1 Failure mechanism of rotational collapse

$$D = c\omega r_0^2 f_d \tag{5}$$

where f_d is the function coefficient of θ_0, θ_h, φ. The detailed expressions of f_w, f_s, and f_d are given in the Appendix.

Substituting Eqs. (3)-(5) into Eq. (2) can obtain the seismic acceleration coefficient k, as

$$k = \frac{cf_d}{\gamma s r_0} - \frac{f_w}{f_s} \tag{6}$$

The upper bound of the yield acceleration k_y is determined through the search for the minimum of k using Eq. (6), and the most critical slip surface is also obtained. After determining k_y, the derived sliding body ABC is discretized into n blocks. For arbitrarily arbitrary nested block i, the corresponding slip surface $(AC)_i$ starts from point A_i and exits the slope face on point C_i. To avoid overlapped blocks, this procedure assumes that point A_i is in the front of the beginning point of the adjacent slip surface which is below the block i and point C_i is above the exiting point of that block. Repeating Eq. (6) can obtain the yield accelerations and geometry of the rest of the nested blocks. In this study, all the mentioned variables with subscript i correspond to block i.

The relative displacement of an arbitrary block i can be evaluated by combining the corresponding yield acceleration k_{yi} and the input of acceleration-time history $k_i(t)$ that is computed through dynamic analysis corresponding to the given block, following the decoupled theorem. This process is presented as follows.

In the arbitrary block i, the movement triggered by seismic forces is assumed as rotational collapse. Hence, an additional work rate of the rotation of the sliding body $\frac{G_i}{g} l_i \ddot{\theta}_i$ will appear as a term on the right side of Eq. (2)

$$\gamma r_{0i}^3 \left[f_i + k_i(t) f_{si} \right] = c r_{0i}^3 f_{di} + \frac{G_i}{g} l_i \ddot{\theta}_i \tag{7}$$

where $\ddot{\theta}$ = the rotation acceleration; G_i = the weight of the rotation block; l_i = the distance from center O_i to the gravity center of the rotation block; and g = the constant of gravity acceleration. The detailed expressions of G_i, l_i are given in the Appendix. The rotation acceleration-time history is solved as

$$\ddot{\theta}_i(t) = \left[k_i(t) - k_{yi} \right] \frac{\gamma r_{0i}^3}{\frac{G_i}{g} l_i^2} f_{si} \tag{8}$$

In terms of the Newmark theorem, the rotation velocity $\ddot{\theta}$ increases as long as $k_i(t)$ exceeds k_{yi} and reaches its maximum when $k_i(t)$ decreases again to k_{yi}. When $k_i(t)$ drops down to some value below k_{yi}, the block slows down and ceases. Double integrating $\ddot{\theta}_i$ over the time interval with a triangle transform, the horizontal relative displacement u_{xi}, which occurs at point C_i, can be calculated.

$$u_{xi}(t) = r_{hi} \sin\theta_{hi} \iint \ddot{\theta}_i \mathrm{d}t\mathrm{d}t \tag{9}$$

Based on Seed and Martin's (1966) theorem, a dynamic analysis is performed to provide the acceleration-time history $k_i(t)$ independently for the decoupled calculation of relative displacements. In the 1-D analysis, $k_i(t)$ can be easily calculated by $k = \tau/\sigma$, where τ is the shear stress at a given height, and σ is the total vertical stress at a given height. The max seismic coefficient at a given height $[k_{max}(h)]$ defines the maximum equivalent loading for a given input motion along the height. Using the one-dimensional site response analysis program – DEEPSOIL (Hashash *et al*., 2016), the dynamic analysis of soil slopes in this study is performed to provide a corresponding acceleration-time history $k_i(t)$ to evaluate the relative displacement u_{xi}. DEEPSOIL is a widely used program in 1-D site response analysis that can perform: 1-D nonlinear time domain analyses with and without pore water pressure generation; 1-D equivalent linear frequency analyses including convolution and deconvolution; and 1-D linear time and frequency domain analyses. To simplify this procedure in this study, 1-D linear frequency domain analyses of DEEPSOIL are used to calculate the response acceleration and shear stress distribution to provide the acceleration-time history $k_i(t)$. The parameters such as H, γ, V_s, and λ should be input, where V_s is the shear wave velocity of a soil column and λ is the damping ratio.

The total horizontal displacement of each nested block is then integrated for a given time increment, starting with the basal region and sequentially proceeding towards the crest (see Fig. 2).

$$d_H = \int_0^H u_{xi}(t) \mathrm{d}H \tag{10}$$

Furthermore, yield accelerations of the upper nested blocks increase as the height increases. Therefore, the upper regions may not encounter yield and their displacement is solely a result of displacement of underlying failures.

3 Verifications

Following the same example given by Leshchinsky (2018), a 1:1 slope (Fig. 3(a) is built on a rigid base, consisting of a uniform soil characterized by γ = 20 kN/m^3, φ = 34° and c = 15 kPa. The dynamic properties of the soil are preestablished with a constant shear wave velocity V_s = 640 m/s and damping ratio λ = 0.2. The

slope is subjected to a seismic input of the 1999 Chi-Chi earthquake in Taiwan (M = 7.52, Station TCU072-000, t = 66 s, Δt = 0.005 s, the vertical acceleration is ignored) scaled to the maximum horizontal acceleration of 0.4 g, as shown in Fig. 3(b). Conducting the presented method can obtain the yield acceleration along the slope height, as illustrated in Fig. 4(a). They are in good agreement with the results given by Leshchinsky (2018).

Using the same input parameters into DEEPSOIL, the 1D dynamic analysis of the slope is carried out to calculate the maximum accelerations of the equivalent seismic loading along slope height, $k_{max}(h)$, as shown in Fig. 4(b). Different from a constant value of the k_{max} using in Leshchinsky (2018), the value of k_{max} derived from the dynamic analysis increases along the height due to the effect of seismic amplification in layered soil. The acceleration k_{max} can reach 0.6 g on the crest of the slope. Based on NNM, 10 evenly-spaced nested blocks are applied to estimate the post-earthquake displacement. Using the yield curve and the equivalent acceleration-time history, the horizontal relative displacement of the series of nested blocks can be calculated. By integrating the relative displacement of each block from toe to crest, the horizontal displacement profile is determined, as shown in Fig. 5. Figure 6 also illustrates the total displacement time-series and initial/deformed slope profiles. Although the seismic amplification towards the crest of the slope is 1.5 times, the calculated total displacement is slightly larger than that of Leshchinsky (2018). The results of decoupled/coupled and rigid block analysis, which are obtained by SLAMMER, are also illustrated in Fig. 6. The maximum displacements are 41.85 cm and 39.62 cm for the decoupled and coupled methods, respectively. They are greater than that of the rigid block analysis (29.90 cm), but are much smaller than the NNM result.

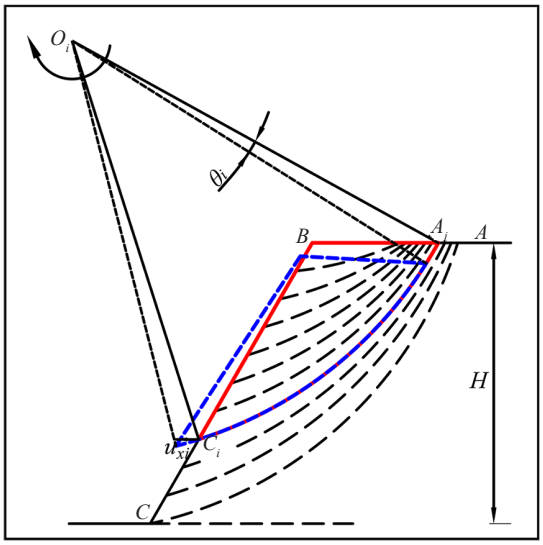

Fig. 2 Displacement pattern of rotational collapse

4 Parametric studies

Using the extended NNM approach, parametric studies (e.g., slope height, shear stiffness, and input motion) are given here to investigate their influences on the post-earthquake displacement profiles of earth slopes.

(1) Slope Height

For homogeneous slopes comprised of the soil properties γ = 20 kN/m^2, c = 20 kPa, φ = 33.8° and λ = 0.2, V_s = 300 m/s and the inclination β = 45°, the slope height can affect the seismic stability according to both the pseudo-static analysis and dynamic response analysis. Different heights H = 20 m, 30 m and 40 m are considered here and then the corresponding yield accelerations for the critical failure are calculated as k_y = 0.21, 0.14 and 0.07, respectively. Based on the obtained critical slip surface, the yield acceleration along the slope height can be determined, as shown in Fig. 7(a). As expected, the yield acceleration increases with the increasing height. DEEPSOIL is used to obtain the maximum acceleration along the slope height with the Chi-Chi seismic input, as illustrated in Fig. 7(b). The amplification of the maximum acceleration on the crest increases from 1.53 to 1.74 as the slope height increases.

As presented in Huang *et al.* (2009), the ratio of the seismic horizontal displacement and the slope height (d_H/H) is given along the height, as shown in Fig. 8. The results derived from the method proposed

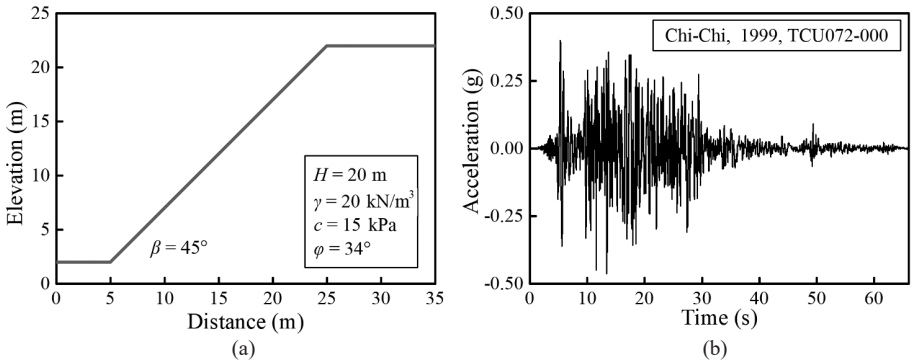

Fig. 3 Example and input motion: (a) slope geometry and soil properties; (b) input seismic motions

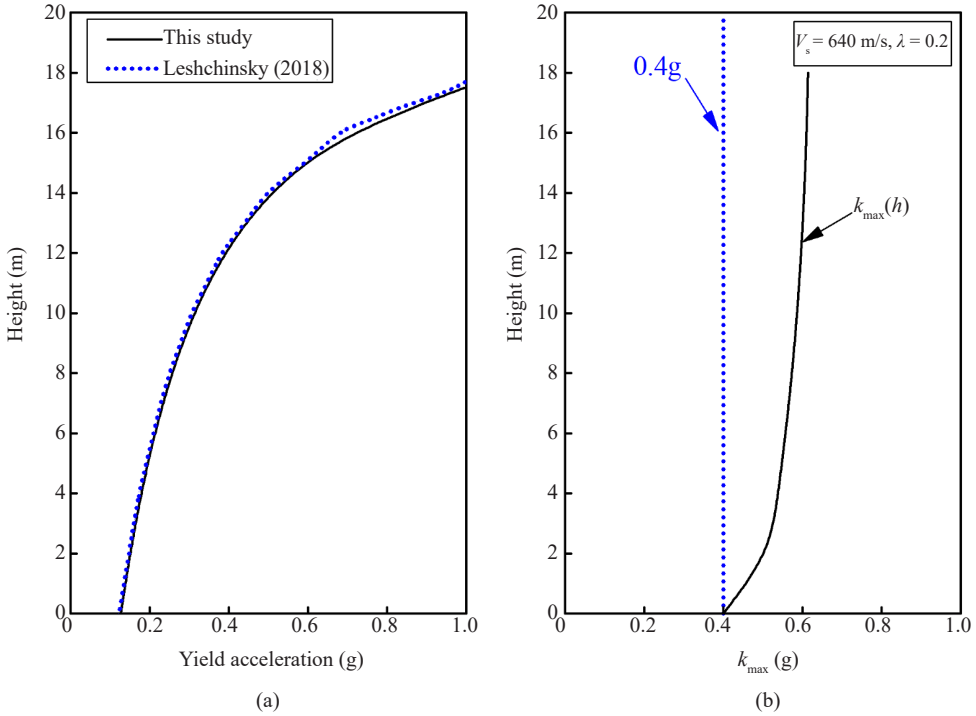

Fig. 4 Comparison of yield acceleration and maximum seismic acceleration: (a) yield curve; (b) maximum seismic accelerations along the slope height

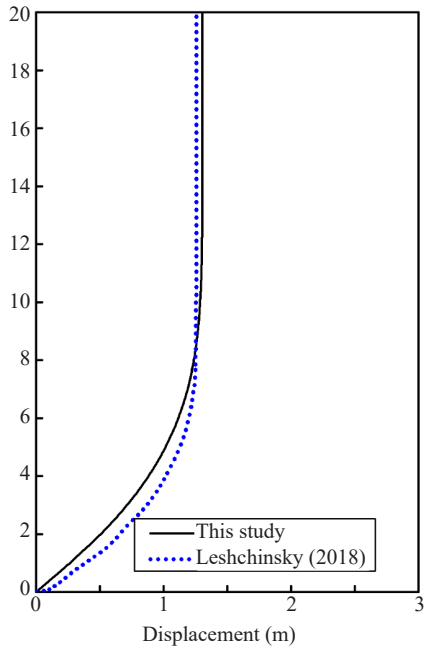

Fig. 5 Horizontal displacement profiles from this study and Leshchinsky (2018)

by Leshchinsky (2018) are also included here for comparison to demonstrate the significant influence of the dynamic response on the seismic displacement. More seismic displacements are induced in slopes with a greater value of height. Figure 9 illustrates the post-earthquake profiles for slopes with different values of height. The dynamic response makes the higher slope unstable, producing larger seismic deformations. Rigid block and decoupled/coupled analysis are also conducted by SLAMMER for comparison, and these results are filled in Table 1. The method of this study yields the greatest value of the seismic displacement. For slope height H = 20 m, the result of NNM method is closer to the results of the decoupled and coupled methods. However, as the slope height increases, the difference becomes significant.

(2) Shear wave velocity

As previously stated, the shear stiffness is characterized by the shear wave velocity V_s. The value of V_s can be estimated by $V_s = \sqrt{G_{max} / \rho}$, where G_{max} = the maximum shear modulus and ρ = soil density. A slope is comprised of H = 35 m, β = 45°, c = 20 kPa, φ = 33.8° and λ = 0.2. Different shear wave velocities V_s = 200 m/s, 300 m/s, 400 m/s, and 500 m/s are considered here for the investigations. The yield accelerations of nested blocks are calculated first using DEEPSOIL and the Chi-Chi seismic wave to obtain the maximum acceleration, as shown in Fig. 10(a). As the shear wave velocity increases, the effect of the seismic amplification becomes less significant on the slope crest. Typically, the amplification of the maximum acceleration decreases from 1.91 times to 1.59 times when the shear wave velocity increases from 100 m/s to 500 m/s. The seismic displacement is calculated along the slope height, as shown in Fig. 10(b). The displacement increases as the shear wave velocity decreases. The maximum displacement derived from the present method occurs at the positions of 28 m for V_s = 500 m/s, while the maximum displacement determined by NNM occurs at a height of 17.5 m. Figure 11

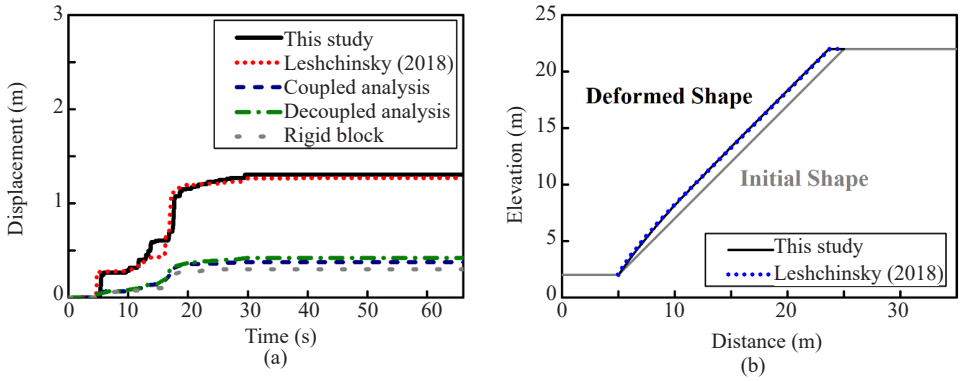

Fig. 6 Comparisons of the displacements of different Newmark methods: (a) displacement time-series; (b) initial/deformed slope profiles

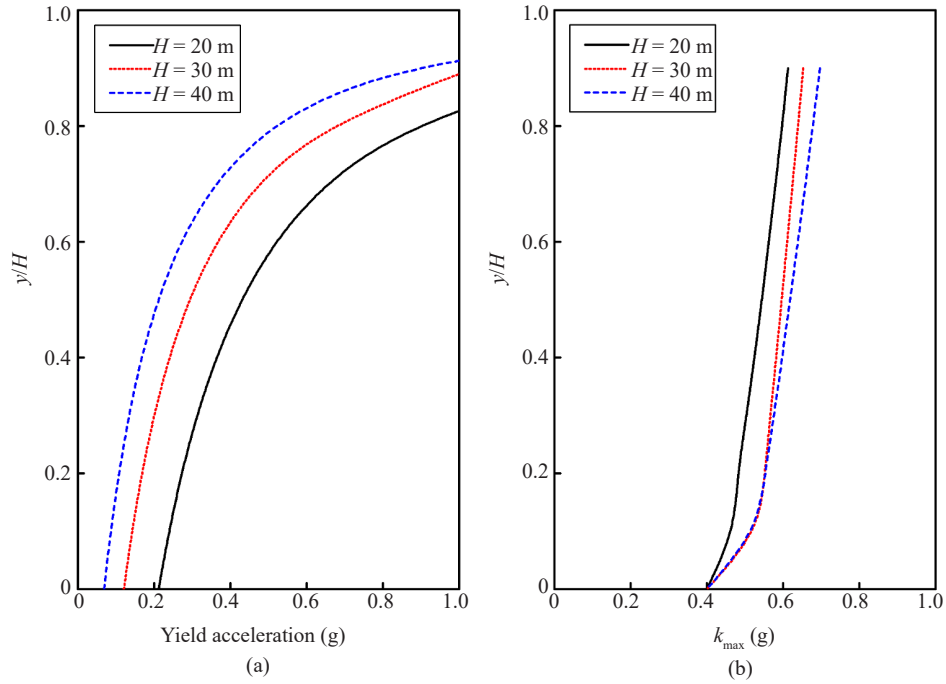

Fig. 7 Yield acceleration and maximum acceleration: (a) yield curve; (b) k_{max} along the slope height from 1D dynamic analysis

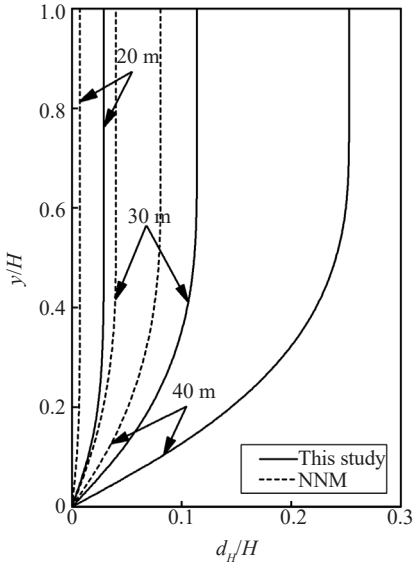

Fig. 8 Horizontal displacement profiles

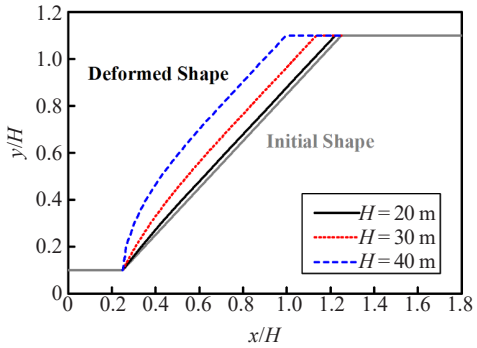

Fig. 9 Initial/deformed slope profiles

illustrates the post-earthquake profiles for slopes with different shear wave velocities. It indicates that ignoring the dynamic response could underestimate the seismic deformation. The post-earthquake deformation becomes more obvious as the shear wave velocity decreases.

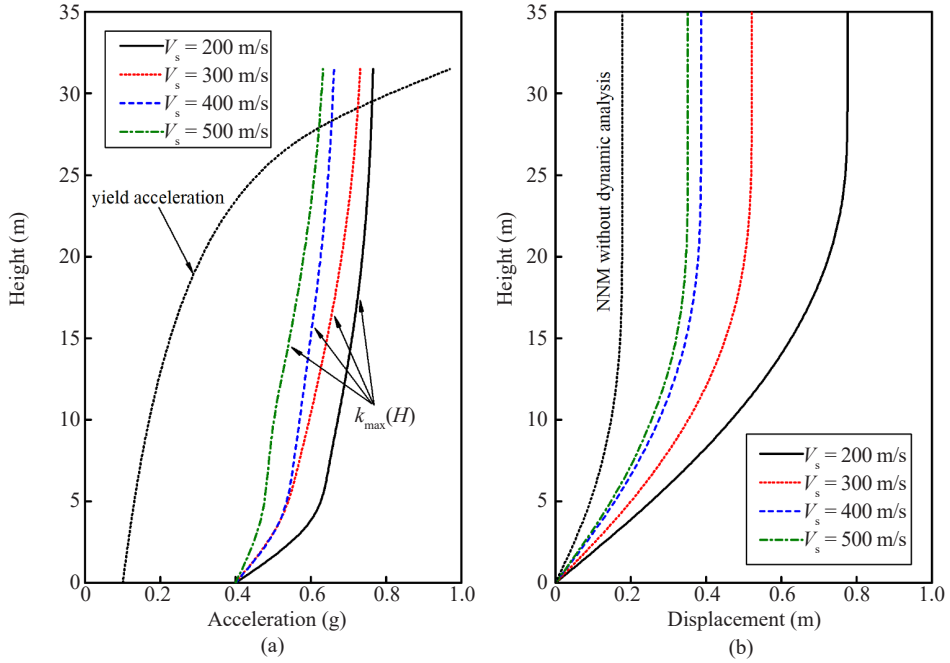

Fig. 10 Influence of soil shear wave velocity: (a) yield curve and maximum seismic accelerations along the slope height; (b) horizontal displacement profiles

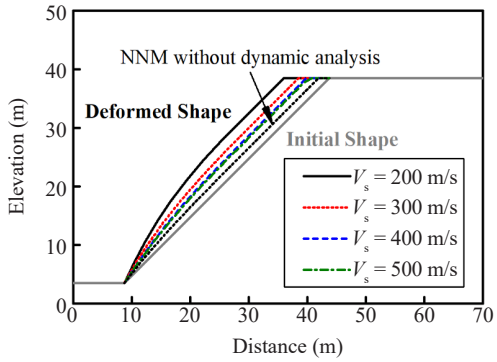

Fig. 11 Initial/deformed slope profiles

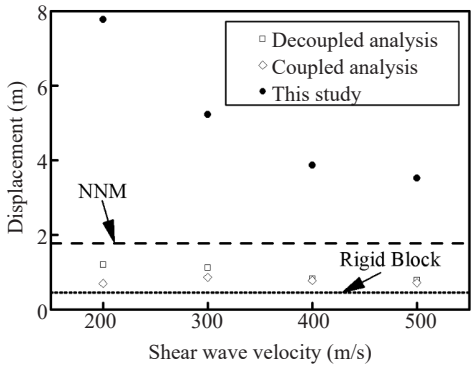

Fig. 12 Effects of the shear wave velocity on the seismic displacement using various Newmark methods

The NNM proposed by Leshchinsky (2018) and the Newmark method based on a rigid block neglect the soil dynamic response. Once the soil dynamic response is involving in Newmark methods, the shear wave will affect the displacements, as shown in Fig. 12. The results of the decoupled/coupled methods are also included. It can be seen that, the effects of the dynamic response become more significant as the shear wave velocity decreases. In addition, the results of decoupled/coupled method are in the range between results of Newmark rigid-block and NNM methods. Therefore, the shear stiffness should be paid more attention to the seismic design of slope stability for practice.

(3) Input Ground Motion

Two selected earthquake records are used here as input into both the present analysis and the NNM. Figure 13 presents the seismic waves for the Chi-Chi and Big Bear earthquakes and two sinusoidal waves, of which the mean period T_m is the same as that for Chi-Chi and Big Bear earthquakes, respectively. The mean period of the Chi-Chi earthquake (T_m = 0.59 s) is greater than that of the Big Bear earthquake (T_m = 0.26 s, 6/26/1992, Civic Center, 90°). The mean period T_m of an earthquake ground motion is defined as follows:

$$T_m = \frac{\sum_i C_i^2 (1/f_i)}{\sum_i C_i^2} \tag{11}$$

where C_i = square roots of the sum of the squared real and imaginary parts of the positive frequency fast Fourier transform coefficients; and f_i = discrete fast Fourier transform frequencies from 0.25 to 20 Hz.

The maximum acceleration of the sinusoidal motions is identical to that of the earthquakes. The 1D fundamental period of soil slopes, T_s, can be estimated

by $T_s = 4H/V_s$. To further investigate the influence of the dynamic response on the seismic displacement, parameter η is introduced here, as the ratio of the maximum horizontal displacements derived from the present method and the NNM.

Figure 14 illustrates the variation of the displacement ratio η with the period ratio T_s/T_m. The calculated results are fitted by the Gaussian regression. When the fundamental period is closer to the mean period of the input motion, the predicted displacement of the present analysis is much quieter than the displacements derived from NNM. For the sinusoidal motions, their difference can reach the maximum value corresponding to $T_s/T_m = 0.98$ and 0.99 for the two cases. For the earthquake records, the ratio η reaches the maximum value when the values of T_s/T_m are 1.14 and 1.22, respectively. The condition approaches resonance when the input motions are smooth sinusoidal wave motions (i.e., not erratic). Figure 14 also indicates that the range of the ratio η varies with the mean period. When the mean period of the input motion is 0.59 s, neglecting the dynamic response can underestimate the seismic displacement, especially for sinusoidal motions. In Fig. 14(b), the present method would be unconservative when $T_s/T_m > 1.80$ in recorded ground motion or $T_s/T_m > 1.38$ in the sinusoidal wave motion.

The decoupled/coupled analyses are also conducted for the discussion. Parameter η is redefined as the ratio of results obtained by decoupled/coupled analyses and Newmark rigid block analysis here. For slopes subjected to Chi-Chi (1999) earthquake, the η is illustrated in Fig. 15. They are smaller than the ratio obtained by the presented method, as shown in Fig. 14(a). The input ground motion can affect the deformation of the slopes and result in resonance effects. When the fundamental period T_s deviates from the mean period of the input motion comprised of low values of the frequency, the predicted displacement of the present analysis is closer to the result of NNM. In this situation, the influence of the dynamic response can be ignored. When the ratio T_s/T_m is greater than a certain value, the displacement obtained from the present method tends towards being smaller than the result of NNM for input motions comprised of high frequency. The influence of the dynamic response

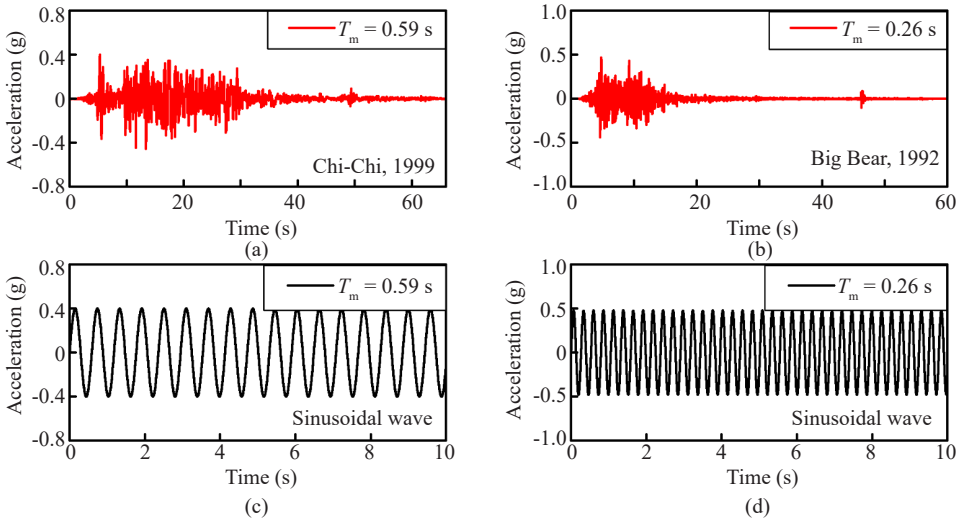

Fig. 13 Input motions: (a) Chi-Chi Earthquake; (b) Big Bear Earthquake; (c) sinusoidal wave (T_m= 0.59 s); (d) sinusoidal wave (T_m= 0.26 s)

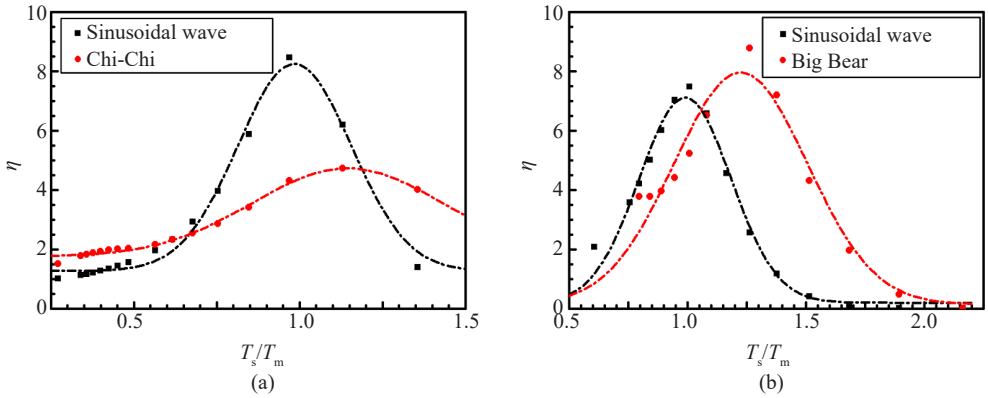

Fig. 14 Effect of input motions: (a) Chi-Chi Earthquake and sinusoidal wave (T_m= 0.59 s); (b) Big Bear Earthquake and sinusoidal wave (T_m= 0.26 s)

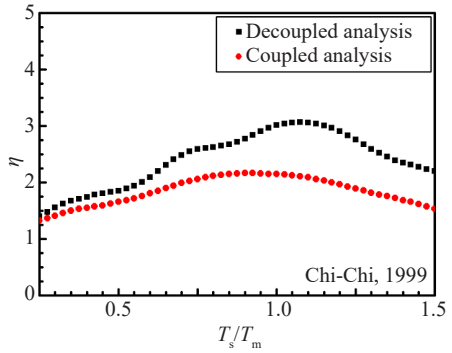

Fig. 15 Ratio η derived from decoupled and coupled methods (Chi-Chi earthquake)

can be ignored when the fundamental period is far away from the mean period of the input motion.

5 Conclusion

This study takes the dynamic response account of NNM to obtain the post-earthquake deformation of slopes in cohesive soils. The rotational log-spiral surface is adopted in LA to determine the upper-bound solution of the yield acceleration. 1D dynamic analysis is carried out in the framework of DeepSoil. Using the decoupled analysis can evaluate the effects of the dynamic response on the seismic slope displacement. Based on the calculated results, the following conclusions can be obtained.

(1) Neglecting the dynamic response can underestimate permanent displacements of the seismic slope.

(2) Involving the dynamic response, the elevation of the maximum displacement is closer to the slope crest. Due to the dynamic response, more nested blocks encounter yield and the deformation becomes more obvious.

(3) When the fundamental period T_s approaches the mean period T_m, the resonance effect is dominant and yields more seismic displacements. For induced earthquake waves with a small value of T_m, the fundamental period deviates from the mean period and then the influence of the dynamic response can be ignored. For high slope comprised of soil with low shear wave velocity, the influence of the dynamic response should not be omitted due to $T_s < T_m$.

As the potential deformed shape and the corresponding maximum deformed region can be obtained from NNM with dynamic analysis, it's useful for seismic design in practice. The presented method neglects the sliding in the dynamic response analysis and is limited to the uniform slopes. For reinforced slopes/walls, their flexible or rigid reinforcements may affect both the failure mechanism and the dynamic response. Extrapolating the application of the present analysis to reinforced structures is straightforward.

Acknolegement

Financial support by the National Natural Science Foundation of China (Grant Nos. 41630638 and 41602280), the National Key Research and Development Program of China (Grant No. 2016YFC0800205), the Program of Introducing Talents of Discipline to Universities (111 Project; Grant No. B13024) is gratefully acknoledged.

Reference

Aminpour MM, Maleki M and Ghanbari A (2018), "Predicting Seismic Permanent Displacement of Soil Walls Under Surcharge Based on Limit Analysis Approach," *Earthquake Engineering and Engineering Vibration*, **17**(4): 747–759.

Baker R and Garber M (1978), "Theoretical Analysis of the Stability of Slopes," *Géotechnique*, **28**(4): 395–411.

Bouckovalas GD and Papadimitriou AG (2005), "Numerical Evaluation of Slope Topography Effects on Seismic Ground Motion," *Soil Dynamics and Earthquake Engineering*, **25**(7-10): 547–558.

Chugh AK and Stark TD (2006), "Permanent Seismic Deformation Analysis of a Landslide," *Landslides*, **3**(1): 2–12.

Dai D, Zhang N, Lee VW, Gao Y and Chen X (2019), "Scattering and Amplification of SV Waves by a Semi-Cylindrical Hill in a Half-Space by a Wavefunction-Based Meshless Method Using Mapping and Point-Matching Strategies," *Engineering Analysis With Boundary Elements*, **106**: 252–263.

Goodman PE and Seed HB (1966), "Earthquake-Induced displacements in Sand Embankments," *Journal of Soil Mechanics & Foundations Div*, **92**(2): 125–146.

Hashash YMA, Musgrove MI, Harmon JA, Groholski DR, Phillips CA and Park D (2016), *DEEPSOIL 6.1, User Manual*, Urbana, IL, Board of Trustees of University of Illinois at Urbana-Champaign.

Hong Y-S, Chen R-H, Wu C-S and Chen J-R (2005), "Shaking Table Tests and Stability Analysis of Steep Nailed Slopes," *Canadian Geotechnical Journal*, **42**(5): 1264–1279.

Huang CC, Wu SH and Wu HJ (2009), "Seismic Displacement Criterion for Soil Retaining Walls Based on Soil Strength Mobilization," *Journal of Geotechnical and Geoenvironmental Engineering*, **135**(1): 74–83.

Jibson RW (2011), "Methods for Assessing the Stability of Slopes During Earthquakes—A retrospective," *Engineering Geology*, **122**(1–2): 43–50.

Kutter B and James R (1989), "Dynamic Centrifuge Model Tests on Clay Embankments," *Géotechnique*, **39**(1): 91–106.

Lee KL (1974). *Seismic Permanent Deformations in*

Earth Dams, Report No. UCLA-ENG-7497, School of Engineering and Applied Science, University of California at Los Angeles.

Leshchinsky BA (2018), "Nested Newmark Model to Ealculate the Post-Earthquake Profile of Slopes," *Engineering Geology*, **233**: 139–145.

Leshchinsky D, Baker R and Silver ML (1985), "Three Dimensional Analysis of Slope Stability," *International Journal for Numerical and Analytical Methods in Geomechanics*, **9**(3): 199–223.

Lin M-L and Wang K-L (2006), "Seismic Slope Behavior in a Large-Scale Shaking Table Model Test," *Engineering Geology*, **86**(2–3): 118–133.

Ling HI and Leshchinsky D (1995), "Seismic Performance of Simple Slopes," *Soils and Foundations*, **35**(2): 85–94.

Makdisi FI and Seed HB (1978), "Simplified Procedure for Estimating Dam and Embankment Earthquake-Induced Deformations," *Journal of Geotechnical and Geoenvironmental Engineering*, **104**.

Newmark NM (1965), "Effects of Earthquakes on Dams and Embankments," *Géotechnique*, **15**(2): 139–160.

Rathje EM and Bray JD (2001), "One-and Two-Dimensional Seismic Analysis of Solid-Waste Landfills," *Canadian Geotechnical Journal*, **38**(4): 850–862.

Sarma SK and Bhave MV (1974), "Critical Acceleration Versus Static Factor of Safety in Stability Analysis of Earth Dams and Embankments," *Géotechnique*, **24**(4): 661–665.

Sarma SK (1975), "Seismic stability of earth dams and embankments," *Géotechnique*, **25**(4): 743–761.

Seed HB, Idriss IM, Lee KL and Makdisi FI (1975), "Dynamic Analysis of the Slide in the Lower San Fernando Dam during the Earthquake of February 9, 1971," *Journal of Geotechnical and Geoenvironmental Engineering*, **101**(9): 889–911.

Serff N, Seed HB, Makdisi FI and Chang CY (1976), Earthquake-Induced Deformations of Earth Dams, Report EERC 76-4. *Earthquake Engineering Research Center*, University of California, Berkeley.

Terzaghi K (1950), *Mechanisms of landslides. Engineering Geology* (*Berkey*) *Volume*, Geological Society of America.

Wartman J, Seed RB and Bray JD (2005), "Shaking Table Modeling of Seismically Induced Deformations in Slopes," *Journal of Geotechnical and Geoenvironmental Engineering*, **131**(5): 610–622.

Yang S, Leshchinsky B, Cui K, Zhang F and Gao Y "Influence of Failure Mechanism on Seismic Bearing Capacity Factors for Shallow Foundations Near Slopes," *Géotechnique*, **0**(0): 1–14. http://doi.org/10.1680/jgeot.19.P.329

You L and Michalowski RL (1999), "Displacement Charts for Slopes Subjected to Seismic Loads," *Computers and Geotechnics*, **25**(1): 45–55.

Zhang Ning, Gao Yufeng, Wu Yongxin and Zhang Fei (2018), "A Note on Near-Field Site Amplification Effects of Ground Motion from a Radially Inhomogeneous Valley," *Earthquake Engineering and Engineering Vibration*, **17**(4): 707–718. https://doi.org/10.1007/s11803-018-0470-9.

Appendix

$$W_\gamma = \gamma\omega r_0^3\left(f_{w1} - f_{w2} - f_{w3}\right) = \gamma\omega r_0^3 f_w$$

$$f_{w1} = \frac{\exp[3(\theta-\theta_0)\tan\varphi]\left(3\tan\varphi\cos\theta_\mathrm{h} + \sin\theta_\mathrm{h}\right) - 3\tan\varphi\cos\theta_0 - \sin\theta_0}{3\left(1+9\tan^2\varphi\right)}$$

$$f_{w2} = \frac{L}{6r_0}\sin\theta_0\left(2\cos\theta_0 - \frac{L}{r_0}\right)$$

$$f_{w3} = \frac{1}{6}\exp\left[\left(\theta_\mathrm{h}-\theta_0\right)\tan\varphi\right]\left[\sin\left(\theta_\mathrm{h}-\theta_0\right) - \frac{L}{r_0}\sin\theta_\mathrm{h}\right]\cdot \left\{\cos\theta_\mathrm{h} - \frac{L}{r_0} + \cos\theta_\mathrm{h}\exp\left[\left(\theta_\mathrm{h}-\theta_0\right)\tan\varphi\right]\right\}$$

$$W_s = \gamma\omega r_0^3\left(f_{s1} - f_{s2} - f_{s3}\right) = \gamma\omega r_0^3 f_s$$

$$f_{s1} = \frac{\left\{\left(3\tan\varphi\sin\theta_\mathrm{h} - \cos\theta_\mathrm{h}\right)\exp\left[3\left(\theta_\mathrm{h}-\theta_0\right)\tan\varphi\right] - 3\tan\varphi\sin\theta_0 + \cos\theta_0\right\}}{3\left(1+9\tan^2\varphi\right)}$$

$$f_{s2} = \frac{L}{3r_0}\sin^2\theta_0$$

$$f_{s3} = \frac{1}{6}\left\{\sin\theta_0 + \sin\theta_\mathrm{h}\exp\left[\left(\theta_\mathrm{h}-\theta_0\right)\tan\varphi\right]\right\}\cdot \left[\sin\left(\theta_\mathrm{h}-\theta_0\right) - \frac{L}{r_0}\sin\theta_\mathrm{h}\right]$$

$$f_{di} = \frac{\exp\left[2\left(\theta_\mathrm{h}-\theta_0\right)\tan\varphi\right] - 1}{2\tan\varphi}$$

$$G_i = G_{(ABC)_i} = G_{(AOC)_i} - G_{(AOB)_i} - G_{(BOC)_i}$$

$$G_i = \frac{1}{2}\gamma r_0^2\left\{\frac{\exp\left[2\left(\theta_\mathrm{h}-\theta_0\right)\tan\phi\right] - 1}{2\tan\phi} - \frac{L_i}{r_0}\sin\theta_0 - \frac{H}{r_0}\frac{\sin\left(\beta+\theta_\mathrm{h}\right)}{\sin\beta}\exp\left[\left(\theta_\mathrm{h}-\theta_0\right)\tan\phi\right]\right\}$$

$$l_i = \frac{\gamma r_0^3}{G_i}\sqrt{f_i^2 + f_{si}^{\ 2}}$$